Available online at www.sciencedirect.com

ScienceDirect

Ceramics International 40 (2014) 2467–2475

CERAMICS INTERNATIONAL

www.elsevier.com/locate/ceramint

Photoluminescence imaging of $EuBO_3$, $TbBO_3$, Eu(III)-BO_x, and Tb(III)-BO_x nanostructures

Youngku Sohn*

Department of Chemistry, Yeungnam University, Gyeongsan, Gyeongbuk 712-749, South Korea

Received 21 June 2013; received in revised form 4 August 2013; accepted 4 August 2013
Available online 11 August 2013

Abstract

$EuBO_3$, $TbBO_3$, Eu(III) and Tb(III)-doped boron oxide compounds with Ln (Eu and Tb)/B molar ratios of 1/10 and 1/1 were synthesized by a hydrothermal method and their morphologies, crystal structures and spectral properties were examined by scanning electron microscopy (SEM), X-ray diffraction crystallography, UV–visible absorption, and photoluminescence spectroscopy. 2D and 3D-photoluminescence image profiles of Eu(III) were observed between 570 and 720 nm, and were attributed to the $^5D_0 \rightarrow {}^7F_J$ ($J=0,1,2,3,4$) transition, while emission peaks of Tb(III) between 450 and 700 nm corresponded to the $^5D_4 \rightarrow {}^7F_J$ ($J=6,5,4,3$) transition. Overall, this study describes a method of understanding photoluminescence mechanism and developing efficient phosphor materials using borate compounds.

Keywords: $EuBO_3$; $TbBO_3$; Photoluminescence image; UV–vis absorption; X-ray diffraction

1. Introduction

Lanthanide borates ($LnBO_3$) have attracted increasing attention in recent years due to their chemical stability, vacuum UV transparency, and ability to act as good luminescent host materials [1–6]. Borates with different morphologies have been synthesized by various methods including hydrothermal, solvothermal and sol–gel methods [7–20]. Corbel et al. synthesized triclinic $EuBO_3$ by a solid state reaction and reported detailed crystal structures and sharp luminescence profiles measured at 77 K and 12 K [8]. Velchuri et al. prepared non-uniform micron sized rare earth orthoborates, $LnBO_3$ (Ln=Tb, La, Pr, Nd, Sm, Eu, Gd, Dy, Y), via a metathesis reaction and characterized their properties by powder X-ray diffraction and FT-IR spectroscopy [6]. Uniform micron size $LnBO_3$ (Ln=Gd, Nd, Sm, Eu, Tb, and Dy) microplates could be synthesized via hydrothermal conversion from $Ln(OH)_3$ nanorods at a reaction temperature of 180–200 °C [9]. Xu et al. utilized the hydrothermal method to synthesize nest-like, rose-like, cruller-like, and flower-like three-dimensional architectures of Eu(III)-doped YBO_3 by varying the ratios of the added surfactants [10]. Orange-like $LnBO_3$:Eu^{3+} (Ln=Y and Tb) mesocrystals were prepared by a hydrothermal process and reported by Liu et al. [3].

Eu(III) and Tb(III) ions have most commonly been studied as activators for red and green phosphor materials, respectively. To develop phosphors emitting red and green colors, Eu(III) and Tb(III) ions have been doped into $LnBO_3$ as a host material. Jia et al. doped Eu(III) and Tb(III) into a straw-sheaf like $LaBO_3$ host material and observed strong red and green emissions with lifetimes of 1.68 and 2.13 ms, respectively [4]. When guest ions such as Li^+ and Mg^{2+} were introduced, the luminescence for Eu(III)-doped microsphere YBO_3 host material was shown to be enhanced [2]. $TbBO_3$ has been used as a host material for doping various concentrations of Eu(III) ions, which was $Tb_{(1-x)}BO_3$:xEu^{3+} ($x=0$–1) microspheres [12]. By varying the Eu(III) compositions, Yang et al. could tune the luminescent color (green, yellow, orange, to red-orange) and found that the energy was efficiently transferred from Tb(III) to Eu(III) ions in the host material [12].

In the present study, the Ln (Eu and Tb)/B molar ratio was fixed at 0.1 and 1.0 to examine the photoluminescence characteristics of Eu(III) and Tb(III)-doped boron oxide compounds

*Tel.: +82 53 810 2354; fax: +82 53 810 4613.
E-mail address: youngkusohn@ynu.ac.kr

0272-8842/$ - see front matter © 2013 Elsevier Ltd and Techna Group S.r.l. All rights reserved.
http://dx.doi.org/10.1016/j.ceramint.2013.08.022

before and after thermal annealing. When the Ln/B ratio was 1.0, $LnBO_3$ was obtained by thermal annealing. 2D and 3D photoluminescence imaging of the Eu(III) and Tb(III)-doped boron oxide compounds was then performed to elucidate the photoluminescence mechanism, which is a very important step in development of efficient luminescent materials.

2. Material and methods

Eu and Tb borates ($EuBO_3$ and $TbBO_3$) and Eu(III) and Tb(III)-doped (Ln/B molar ratio = 0.1 and 1.0) boron oxide (written as Eu(III)-BO_x and Tb(III)-BO_x) powders (or granules) were synthesized by the hydrothermal method as described below. For compounds with a molar ratio of B/Eu = 1.0 (or B/Tb = 1.0), 10.0 mL of 0.1 M Eu(III) or Tb(III) nitrate solution was mixed with a stoichiometric amount of B_2O_3 (Sigma-Aldrich, 99.98%), after which 15.0 mL of Millipore water was added. Upon complete homogeneous mixing, 1.0 mL of 32% ammonia solution was added to obtain precipitates, after which the solution was transferred to a 125 mL Teflon-lined stainless steel autoclave and reacted in a 210 °C oven for 12 h. The final powder product was centrifuged, fully washed and then dried in an 80 °C oven for further characterization. Samples with an B/Eu (or B/Tb) molar ratio of 0.1 M ratio were obtained by the same procedure under the same conditions. The as-prepared powder samples were annealed at 700 °C for 4 h in a furnace, after which their surface morphology was examined by scanning electron microscopy (SEM, Hitachi SE-4800). In addition, X-ray diffraction (XRD) patterns of the powder samples were measured using a PANalytical X'Pert Pro MPD diffractometer with Cu Kα radiation, while diffuse reflectance absorption spectra were recorded using a Cary5000 UV–visible spectrophotometer, FT-IR spectra were obtained using a Thermo Fisher Scientific iS10 spectrometer and a Scinco FluoroMate FS-2 was utilized to take 2D and 3D-photoluminescence image profiles.

3. Results and discussion

Fig. 1 shows the SEM images of as-prepared and annealed Eu(III)-BO_x samples with B/Eu(III) molar ratios of 10/1 (written as B_{10}/Eu_1) and 1/1 (written as B_1/Eu_1). The as-prepared B_{10}/Eu_1 and B_1/Eu_1 samples showed particle and feather-like morphologies, respectively. Upon annealing, the morphologies of the samples changed distinctively (Fig. 1). Optical microscopy images revealed that the morphologies of the bulk states for the B_{10}/Eu_1 and the B_1/Eu_1 samples were opaque and semitransparent, respectively. Under UV (365 nm) irradiation, the samples emitted red of differing brightness, with the annealed B_{10}/Eu_1 sample generating the brightest color.

Fig. 2 shows the SEM images of as-prepared and annealed Tb(III)-BO_x (B_{10}/Tb_1 and B_1/Tb_1) samples. Changes in morphology were observed after annealing as for the B/Eu samples. The morphologies for the bulk states were very similar to those of the B/Eu samples. For the B/Eu samples, optical microscopy images showed that the B_{10}/Tb_1 and the B_1/Tb_1 samples were opaque and semitransparent, respectively. Under UV irradiation of 365 nm, the Tb(III)-boron oxide compounds emitted a green color, with the brightest color being observed for the as-prepared B_{10}/Tb_1 sample.

Fig. 3 displays the XRD patterns of the as-prepared and annealed and Eu(III)-BO_x (left) and Tb(III)-BO_x (right) samples with B/Ln (Eu, Tb) molar ratios of 10/1 and 1/1. For the as-prepared sample with the molar ratio of B/Eu = 1.0 (B_1/Eu_1), the XRD peak was broad with no characteristic features. However, upon annealing at 700 °C, the XRD showed very clearly sharp patterns that were in good agreement with those of hexagonal $EuBO_3$ (JCPDS 13-0485). Three major peaks at $2\theta = 19.97°$, 26.85° and 33.64° were assigned to the (002), (100), and (102) planes, respectively. Other planes were assigned to the corresponding XRD peaks (Fig. 3). For the sample, when the molar ratio was B/Tb = 1.0 (B_1/Tb_1), the XRD patterns were very similar to those of the B_1/Eu_1 sample. Before annealing, no characteristic features were observed. For the 700 °C annealed sample, the XRD patterns were in good agreement with those of hexagonal $TbBO_3$ (JCPDS 24-1272). Three major peaks were found at $2\theta = 20.24°$, 27.22° and 34.02° and assigned to the (002), (100) and (102) planes, respectively. When compared to the XRD peak positions of $EuBO_3$, slightly larger 2θ values were observed, indicating a smaller d (=lattice plane distance) value, which originated from the smaller ionic radius of Tb(III) than that of Eu(III).

Fig. 4 displays the UV–visible absorption spectra of as-prepared and annealed Eu(III)-BO_x (left) and Tb(III)-BO_x (right) samples with molar ratios of B/Ln (Ln = Eu, Tb) of 10/1 and 1/1. For the Eu(III)-BO_x samples, sharp and small peaks were commonly found between 350 nm and 600 nm. These peaks were attributed to the transitions from the ground state ($^7F_0$) of Eu(III) to excited states such as $^5D_0$, $^5D_1$, $^5D_2$, $^5D_3$, $^5L_6$, and $^5G_6$ [21]. The broad absorption band at 250 nm was attributed to a charge transfer band, which became broader after thermal annealing. For the as-prepared Tb(III)-BO_x samples before annealing, weak peaks were commonly found and assigned to the transitions from the ground state ($^7F_6$) of Tb(III) to excited states such as $^5D_4$, $^5D_3$, $^5L_{10}$ and $^5D_2$ [21]. Upon annealing, the weak peaks of Tb(III) were diminished.

Fig. 5 shows the FT-IR spectra of as-prepared and annealed and Eu(III)-BO_x (left) and Tb(III)-BO_x (right) samples with B/Ln (Ln = Eu, Tb) molar ratios of 10/1 and 1/1. The FT-IR spectra of Eu(III)-BO_x samples were very similar to those of Tb(III)-BO_x samples.

For the as-prepared samples, a broad peak was commonly found at 3400 cm^{-1}, which was ascribed to the OH stretching mode. For the annealed samples with a B/Ln (Ln = Eu, Tb) molar ratio of 1.0 ($EuBO_3$ and $TbBO_3$), the IR peaks between 800 and 1200 cm^{-1} were consistent with those of the vaterite-type borate, and the peak at around 1340 cm^{-1} was attributed to asymmetric stretching of the BO_3 of $LnBO_3$ [16,17].

As shown in the FT-IR spectra, the OH groups are commonly present for both as-prepared and annealed samples. The OH group is known to quench luminescence via non-radiative relaxation processes [22–25]. Therefore, it is very important to eliminate the OH groups for achieving applications to the fields such as optical detectors and light emitting

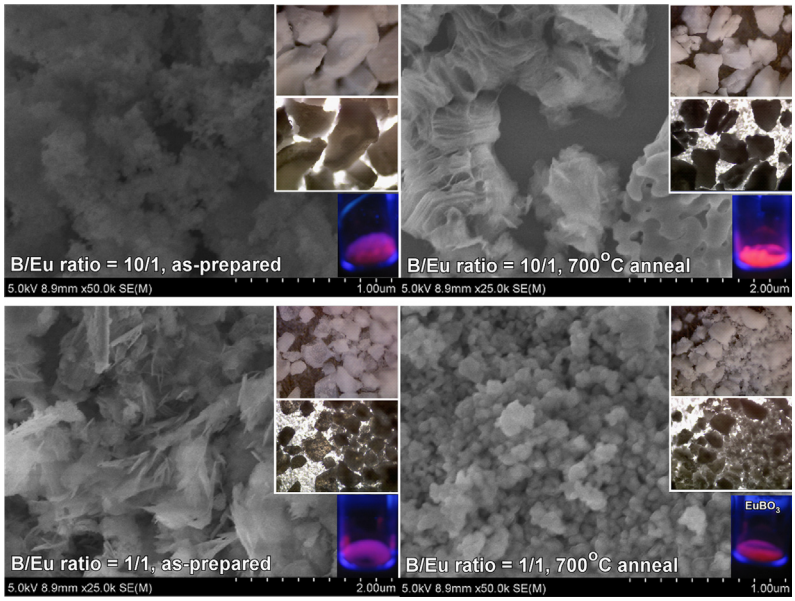

Fig. 1. SEM images of as-prepared and annealed B_{10}/Eu_1 and B_1/Eu_1 samples. Optical microscopy images (with a light source at the top and the bottom) show the morphology of the bulk state. Photos show the color under a UV lamp (365 nm) (For interpretation of the references to color in this figure legend, the reader is referred to the web version of this article.).

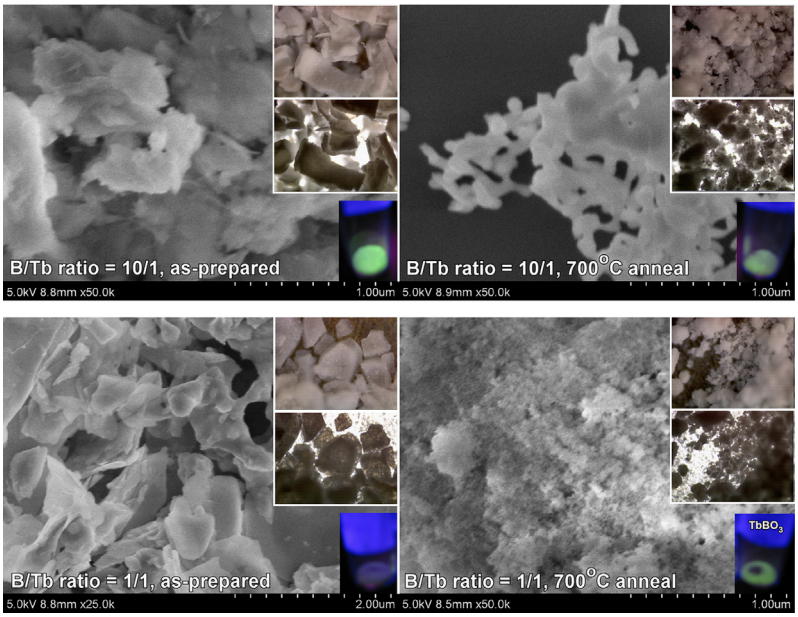

Fig. 2. SEM images of as-prepared and annealed Tb(III)-BO_x (B_{10}/Tb_1 and B_1/Tb_1) samples. Optical microscopy images (with a light source at the top and the bottom) show the morphology of the bulk state. Photo images show the color under a UV lamp (365 nm) (For interpretation of the references to color in this figure legend, the reader is referred to the web version of this article.).

displays [20,22]. The luminescence quenching is plausibly reduced by employing a surface modification technique and synthesizing core–shell type structures [26].

Fig. 6 displays the excitation/emission spectra and the corresponding 2D and 3D-photoluminescence image profiles for the as-prepared (left column) and annealed (right column) Eu(III)-BO_x samples with a B/Eu molar ratio of 10/1. An excitation wavelength of 395 nm was selected to record the emission spectrum from 560 to 720 nm. The excitation wavelength corresponds to the direct $^5L_6 \leftarrow {}^7F_0$ excitation transition of Eu(III) [21]. The emission peaks are associated with the following transitions of the Eu(III) ion: $^5D_0 \rightarrow {}^7F_J$ ($J=0$–4); $^5D_0 \rightarrow {}^7F_0$ (579.4 nm), $^5D_0 \rightarrow {}^7F_1$ (588.7 nm and 594.2 nm), $^5D_0 \rightarrow {}^7F_2$ (614.0 and 622.1 nm), $^5D_0 \rightarrow {}^7F_3$ (652.2 nm), and $^5D_0 \rightarrow {}^7F_4$ (683.9 nm, 692.7 nm, and 700.5 nm) [21]. The dominant emission wavelength of 614 nm ($^5D_0 \rightarrow {}^7F_2$) was chosen to generate an excitation spectrum. Various sharp peaks between 350 nm and 560 nm

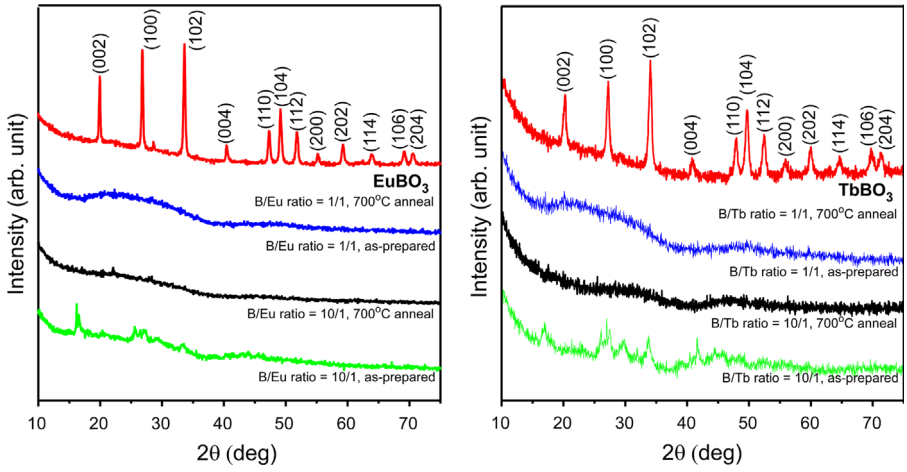

Fig. 3. Power X-ray diffraction patterns of as-prepared and annealed and Eu(III)-BO_x (left) and Tb(III)-BO_x (right) samples with molar ratios of B/Ln (Ln = Eu and Tb) = 10/1 and 1/1.

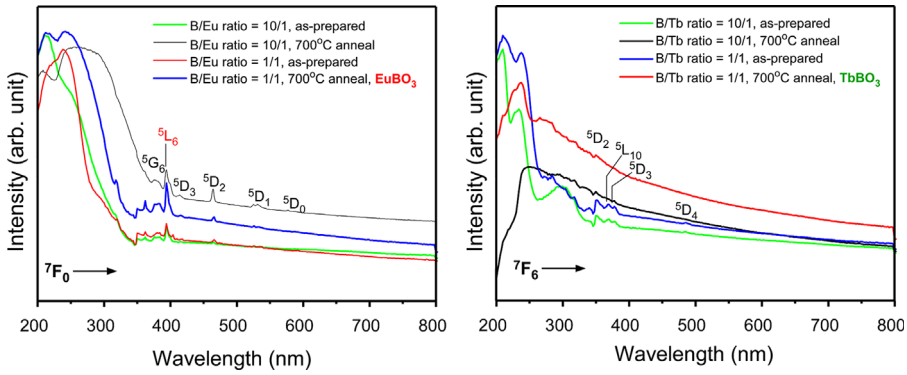

Fig. 4. UV–visible absorption spectra of as-prepared and annealed and Eu(III)-BO_x (left) and Tb(III)-BO_x (right) samples with molar ratios of B/Ln (Ln = Eu and Tb) of 10/1 and 1/1.

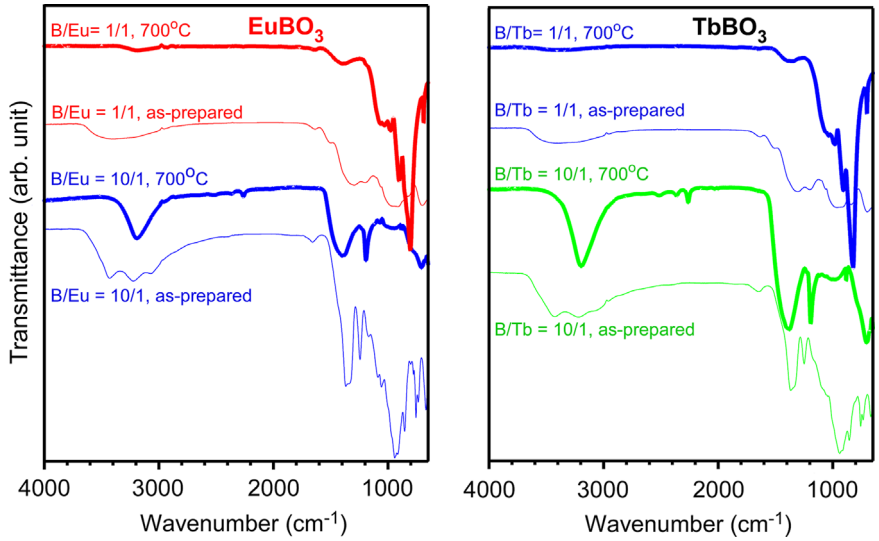

Fig. 5. FT-IR spectra of as-prepared and annealed and Eu(III)-BO_x (left) and Tb(III)-BO_x (right) samples with molar ratios of B/Ln (Ln = Eu and Tb) of 10/1 and 1/1.

were already assigned to the transitions from the ground $^7F_0$ state to the excited states, as shown in the UV–vis absorption spectra (Fig. 4). The broad band below 300 nm was attributed to the Eu^{3+}–O^{2-} charge transfer, which was significantly enhanced upon thermal annealing [20]. The corresponding 2D and 3D photoluminescence image profiles clearly showed the

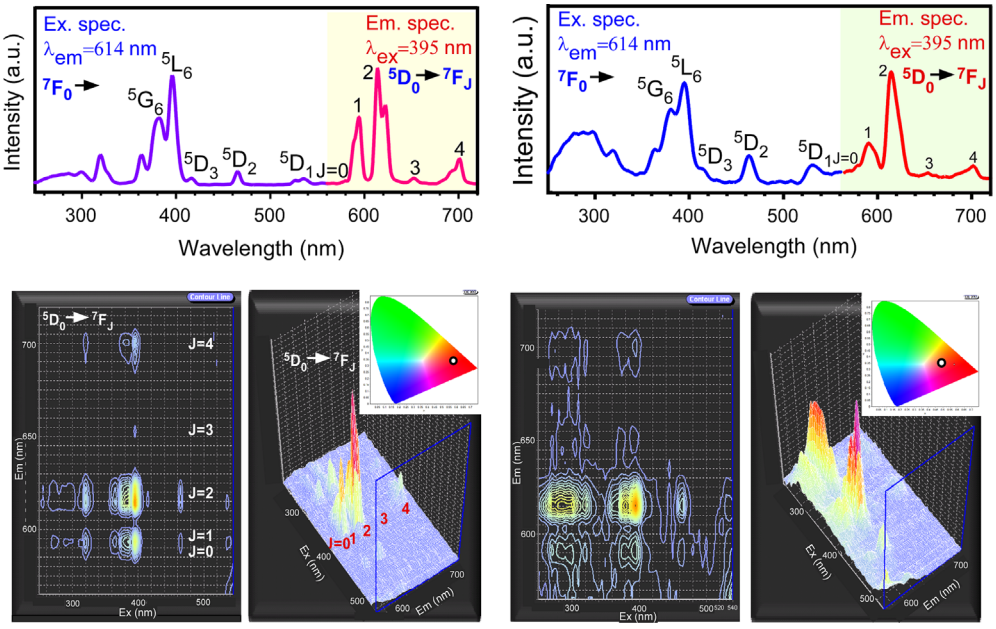

Fig. 6. Excitation/emission spectra (top) and 2D/3D photoluminescence images (bottom) of as-prepared (left column) and annealed (right column) Eu(III)-BO_x samples with a B/Eu molar ratio of 10/1. Insets show the CIE coordinates for the corresponding samples at an excitation wavelength of 395 nm (For interpretation of the references to color in this figure legend, the reader is referred to the web version of this article.).

total excitation and emission characteristics. The Commission Internationale del'Eclairage (CIE) color coordinate obtained at an excitation wavelength of 395 nm was in the red region. The excitation and emission spectra for the annealed sample shown in Fig. 6 (right column) were different from those for the as-prepared samples. These findings indicate that the sites of Eu(III) changed upon thermal annealing. The intensities corresponding to $^5D_2$ and $^5D_2 \leftarrow {}^7F_0$ transitions were somewhat enhanced; however, other transitions from the $^7F_0$ state showed no critical changes in spectral positions or shapes. In the corresponding 2D and 3D photoluminescence image profiles, the emission by an indirect excitation between 250 nm and 300 nm was greatly enhanced. The CIE color coordinate at an excitation wavelength of 395 nm was in the red region, but shifted slightly to the center.

Fig. 7 shows the excitation/emission spectra and the corresponding 2D and 3D-photoluminesce profiles of as-prepared (left column) and annealed (right column) Eu(III)-BO_x samples with a B/Eu molar ratio of 1/1. For the two (left and right) excitation spectra, the peaks could be assigned as described above in Fig. 6. The different emission profiles originated from different local sites of Eu(III), which also depend on the concentration of Eu(III) [7,21]. Upon thermal annealing at 700 °C, the sample showed a crystal structure of $EuBO_3$. Specifically, the broad peak below 350 nm was reduced while the intensities corresponding to the $^5D_2$ and $^5D_2 \leftarrow {}^7F_0$ transitions were greatly enhanced. The two emission profiles were very similar and associated with $^5D_0 \rightarrow {}^7F_J$ (J=0–4) transitions of the Eu(III) ion. The charge transfer band was not significant when compared with that of Eu(III)-BO_x samples with a B/Eu molar ratio of 10/1 (Fig. 6). The CIE color coordinate at an excitation wavelength of 395 nm was located at a much deeper red region than samples with the B/Eu molar ratio of 10/1. As shown in Fig. 7, the chromaticity value was almost the same for the as-prepared and annealed samples.

Fig. 8 redisplays the emission spectra at various excitation wavelengths for the as-prepared and annealed Eu(III)-BO_x samples with B/Eu molar ratios of 10/1 and 1/1. For samples with a molar ratio of 10/1, the emission peak profiles were very similar to the excitation wavelengths, except for the peak intensities. However, for samples with a molar ratio of 1/1, the emission profiles were different, especially for the peak corresponding to the $^5D_0 \rightarrow {}^7F_2$ transition. Two peaks at 613 nm and 625 nm were found at an excitation wavelength of 260 nm. As the excitation wavelength increased, the two $^5D_0 \rightarrow {}^7F_2$ transition peaks merged to a broad peak at 615 nm, while the $^5D_0 \rightarrow {}^7F_1$ transition peak at 593 nm became broader and asymmetric. These findings were likely due to coexistence of two different sites of Eu(III) [18]. Two different photoluminescence profiles could then be expected by the indirect excitation wavelengths below 300 nm and the direct excitation ($\leftarrow {}^7F_0$) transitions [27].

Fig. 9 shows the excitation/emission spectra and the corresponding 2D and 3D-photoluminescence profiles for the as-prepared (left column) and annealed (right column) Tb(III)-BO_x samples with a B/Tb molar ratio of 10/1. An excitation wavelength of 370 nm was selected to record the emission spectrum from 560 to 700 nm. The excitation wavelength corresponds to the direct $^5G_6 \leftarrow {}^7F_6$ excitation transition of Tb (III). The distinctive emission peaks are associated with the following transitions of the Tb(III) ion: $^5D_4 \rightarrow {}^7F_J$ (J=6,5,4,3); $^5D_4 \rightarrow {}^7F_6$ (491 nm), $^5D_4 \rightarrow {}^7F_5$ (544 nm), $^5D_4 \rightarrow {}^7F_4$ (585 nm), and $^5D_4 \rightarrow {}^7F_3$ (623 nm). After thermal annealing at 700 °C, the emission profiles and peak positions showed no critical change. For the excitation spectrum taken at a fixed emission wavelength of 545 nm ($^5D_4 \rightarrow {}^7F_5$), the strong peaks between 300 nm and 400 nm were assigned to the direct $^5L_{10}$, $^5G_6$, $^5D_3 \leftarrow {}^7F_0$ excitation transitions of Tb(III). The excitation

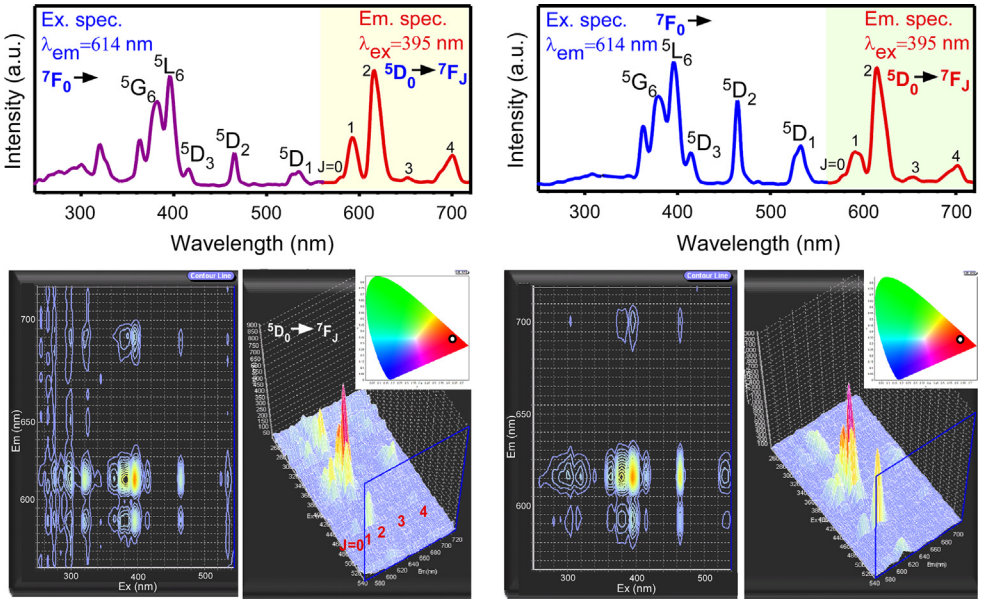

Fig. 7. Excitation/emission spectra (top) and 2D/3D photoluminescence images (bottom) of as-prepared (left column) and annealed (right column) Eu(III)-BO_x samples with B/Eu ratios of 1/1. Insets show the CIE color coordinates for the corresponding samples at an excitation wavelength of 395 nm.

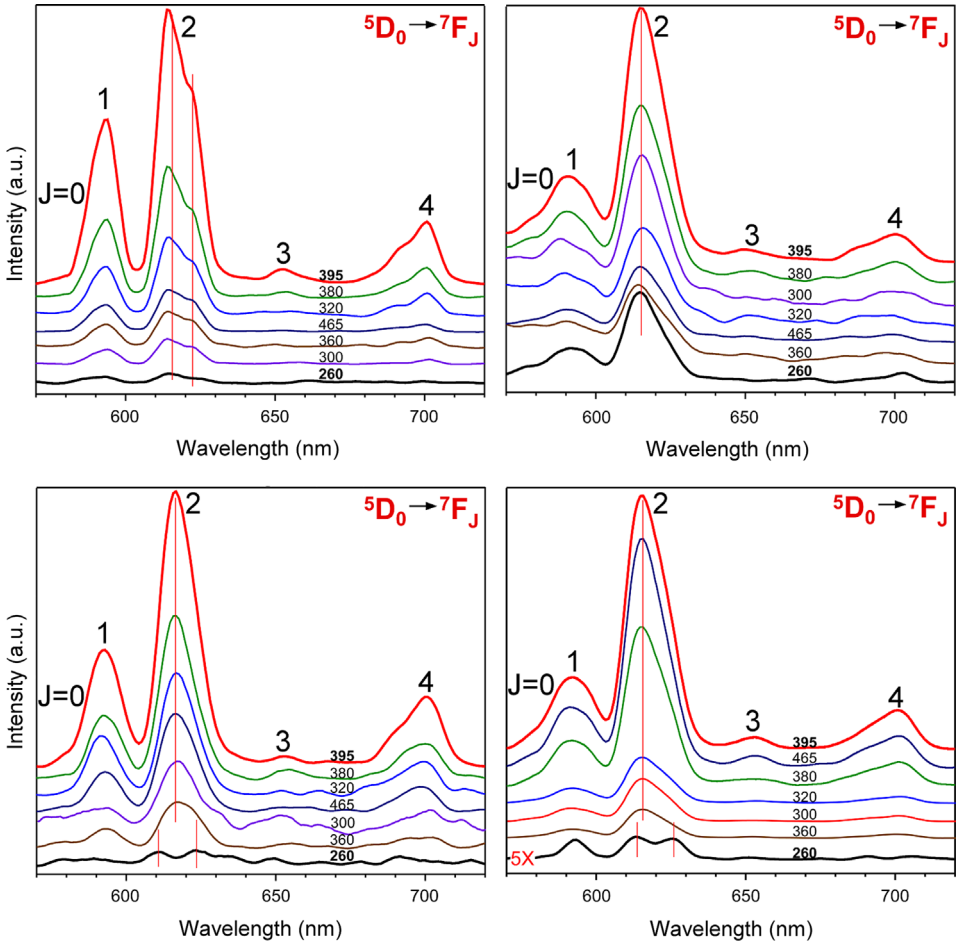

Fig. 8. Emission spectra of as-prepared (left column) and annealed (right column) Eu(III)-BO_x samples with a B/Eu molar ratio of 10/1 (top) and 1/1 (bottom) at various excitation wavelengths.

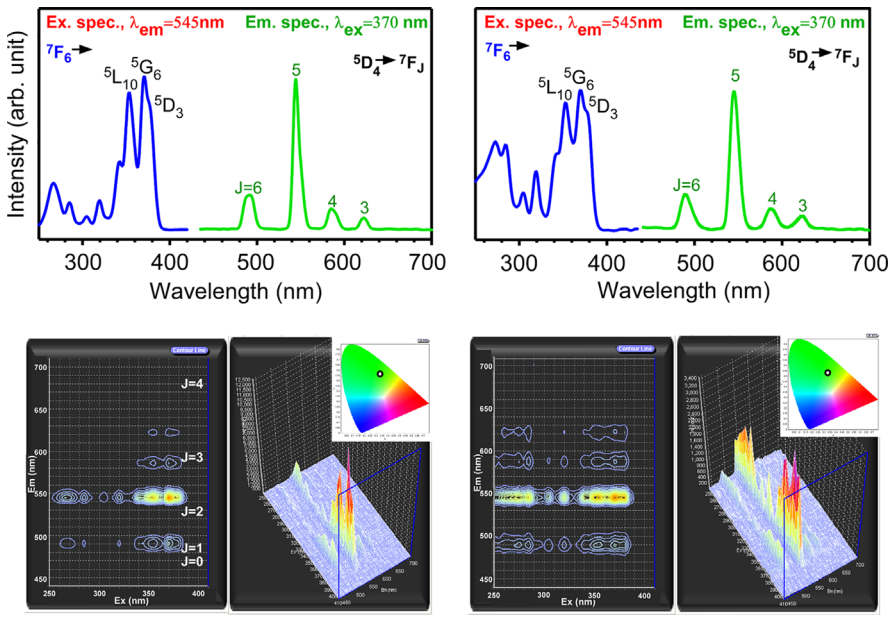

Fig. 9. Excitation/emission spectra (top) and 2D/3D photoluminescence profiles (bottom) of as-prepared (left column) and annealed (right column) Tb(III)-BO_x samples with a B/Tb ratio of 10/1. Insets show the CIE coordinates for the corresponding samples at an excitation wavelength of 370 nm (For interpretation of the references to color in this figure legend, the reader is referred to the web version of this article.).

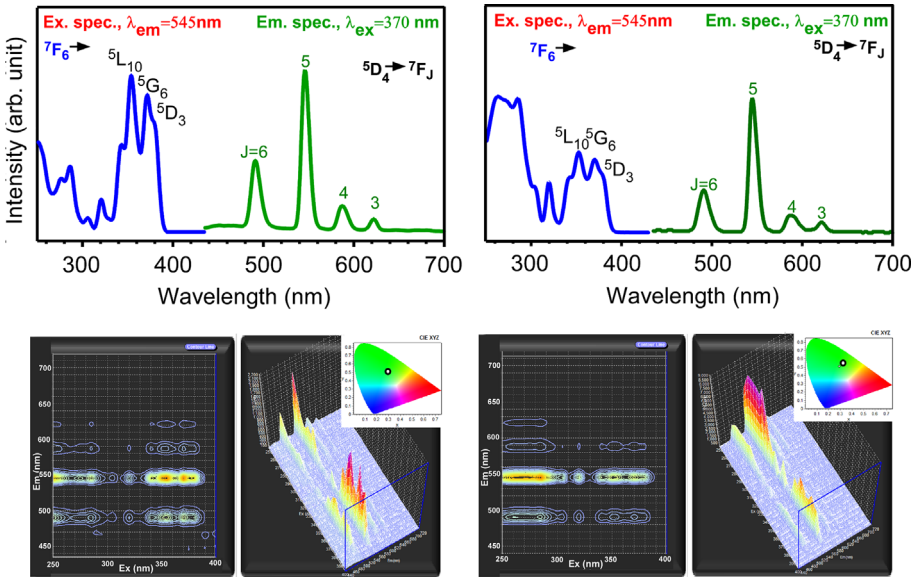

Fig. 10. Excitation/emission spectra (top) and 2D/3D photoluminescence profiles (bottom) of as-prepared (left column) and annealed (right column) Tb(III)-BO_x samples with a B/Tb ratio of 1/1. Insets show the CIE coordinates for the corresponding samples at an excitation wavelength of 370 nm (For interpretation of the references to color in this figure legend, the reader is referred to the web version of this article.).

spectrum showed a significant change below 300 nm after thermal annealing. The broad peak below 300 nm was attributed to the $4f^8 \rightarrow 4f^7 5d^1$ transition of Tb(III) [12,20], which increased significantly after thermal annealing. As expected, the CIE color coordinate obtained at an excitation wavelength of 370 nm was located in the green region.

Fig. 10 shows the excitation/emission spectra and the corresponding 2D and 3D-photoluminescence profiles of as-prepared (left column) and annealed (right column) Tb(III)-BO_x samples with a B/Eu molar ratio of 1/1. The annealed sample showed the crystal structure of $TbBO_3$. The emission peaks were very similar to those of the Tb(III)-BO_x samples with a B/Eu molar ratio of 10/1, but the $(^5D_4 \rightarrow {}^7F_6)/(^5D_4 \rightarrow {}^7F_5)$ was somewhat enhanced for the sample with a molar ratio of 1/1. The emission peaks were associated with the following transitions of the Tb(III) ion: $^5D_4 \rightarrow {}^7F_J$ $(J=6,5,4,3)$; $^5D_4 \rightarrow {}^7F_6$ (491 nm), $^5D_4 \rightarrow {}^7F_5$ (544 nm), $^5D_4 \rightarrow {}^7F_4$ (588 nm), and $^5D_4 \rightarrow {}^7F_3$ (622 nm). For the

excitation spectrum, the $4f^8 \rightarrow 4f^7 5d^1$ transition of Tb(III) below 300 nm increased significantly upon thermal annealing, and this band was much stronger than the peaks between 300 nm and 400 nm. The four different Tb(III)-BO_x samples (Figs. 9 and 10) showed similar CIE color coordinates at an excitation wavelength of 370 nm, and were positioned in the green region.

4. Conclusions

The hydrothermal method was employed to synthesize $EuBO_3$, $TbBO_3$, Eu(III) and Tb(III) containing boron oxide nanostructures with a Ln/B molar ratio of 1.0 and 0.1. The as-prepared and 700 °C annealed samples were characterized by scanning electron microscopy (SEM), X-ray diffraction crystallography, UV–visible absorption, and photoluminescence spectroscopy. When the Ln/B molar ratio was 1.0, hexagonal $EuBO_3$ and $TbBO_3$ could be obtained by annealing at 700 °C, as demonstrated by the XRD patterns. 2D and 3D-photoluminescence image profiles were obtained to fully understand the energy transfer and photoluminescence mechanism of the nanostructures. The Eu(III) containing samples commonly showed various emission peaks between 560 and 720 nm, which were associated with the $^5D_0 \rightarrow {}^7F_J$ (J=0,1,2,3,4) transitions of the Eu(III) ion. For the Tb(III) containing samples, the emission peaks observed between 450 nm and 700 nm were attributed to $^5D_6 \rightarrow {}^7F_J$ (J=6,5,4,3) transitions of the Tb(III) ion. The 2D and 3D photoluminescence imaging profiles provide new insights for the development of efficient phosphor materials using borate compounds.

Acknowledgments

This research was supported by Basic Science Research Program through the National Research Foundation of Korea (NRF) funded by the Ministry of Education, Science and Technology (NRF-2012-005645), and partly by NRF-2011-0018403.

References

[1] J. Yang, H. Zhang, Z. Wang, C. Huang, L. Zou, P. Cai, Y. Zhang, S. Hu, Hydrothermal synthesis and improved luminescent properties of nanosheet-based rare earth orthoborates lantern-like assemblies, Journal of Materials Science 48 (2013) 2258–2267.

[2] D. Jin, J. Yang, X. Miao, L. Wang, L. Wang, Improved photoluminescence property of $YBO_3:Eu^{3+}$ phosphor by structure tailoring, International Journal of Applied Ceramic Technology, 10, 603–609.

[3] S.-S. Liu, D.-K. Ma, Y.–Q. Zhang, P. Cai, X.-A. Chen, S.-M. Huang, Controlled synthesis of orange-like $LnBO_3:Eu^{3+}$ (Ln=Y, Tb) mesocrystals via a facile organic additive-free hydrothermal route, CrystEngComm 14 (2012) 2899–2905.

[4] G. Jia, C. Zhang, C. Wang, L. Liu, C. Huang, S. Ding, Uniform and well-dispersed $LaBO_3$ hierarchical architectures: synthesis, formation, and luminescence properties, CrystEngComm 14 (2012) 579–584.

[5] J. Zhang, M. Yang, H. Jin, X. Wang, X. Zhao, X. Liu, L. Peng, Self-assembly of LaBO3:Eu twin microspheres synthesized by a facile hydrothermal process and their tunable luminescence properties, Materials Research Bulletin 47 (2012) 247–252.

[6] R. Velchuri, B.V. Kumar, V.R. Devi, G. Prasad, D.J. Prakash, M. Vithal, Preparation and characterization of rare earth orthoborates, $LnBO_3$ (Ln=Tb, La, Pr,Nd, Sm, Eu, Gd, Dy, Y) and LaBO3: Gd, Tb, Eu by metathesis reaction: ESR of $LaBO_3$:Gd and luminescence of LaBO3:Tb, Eu, Materials Research Bulletin 46 (2011) 1219–1226.

[7] X. Zhang, A. Marathe, S. Sohal, M. Holtz, M. Davis, L.J. Hope-Weeks, J. Chaudhuri, Synthesis and photoluminescence properties of hierarchical architectures of $YBO_3:Eu^{3+}$, Journal of Materials Chemistry 22 (2012) 6485–6490.

[8] G. Corbel, M. Leblanc, E. Antic-Fidancev, M. Lemaitre-Blaise, J. C. Krupa, Luminescence analysis and subsequent revision of the crystal structure of triclinic L-$EuBO_3$, Journal of Alloys and Compounds 287 (1999) 71–78.

[9] G. Jia, H. You, M. Yang, L. Zhang, H. Zhang, Uniform lanthanide orthoborates $LnBO_3$ (Ln) Gd, Nd, Sm, Eu, Tb, and Dy) microplates: general synthesis and luminescence properties, Journal of Physical Chemistry C 113 (2009) 16638–16644.

[10] Y.-F. Xu, D.-K. Ma, X.-A. Chen, D.-P. Yang, S.-M. Huang, Bisurfactant-controlled synthesis of three-dimensional YBO_3/Eu^{3+}architectures with tunable wettability, Langmuir 25 (2009) 7103–7108.

[11] R. Velchuri, B.V. Kumar, V.R. Devi, K.R. Kumar, G. Prasad, M. Vithal, Low temperature preparation and characterization of $In_{1-x}Ln_xBO_3$ (x=0.0 and 0.05; Ln=Gd, Eu, Dy and Sm): ESR of $In_{0.95}Gd_{0.05}BO_3$ and emission of $In_{0.95}$ $Eu_{0.05}BO_3$, Spectrochimica Acta Part A 74 (2009) 726–730.

[12] J. Yang, C. Zhang, C. Li, Y. Yu, J. Lin, Energy transfer and tunable luminescence properties of Eu^{3+} in $TbBO_3$ microspheres via a facile hydrothermal process, Inorganic Chemistry 47 (2008) 7262–7270.

[13] Y. Li, J. Zhang, X. Zhang, Y. Luo, S. Lu, X. Ren, X. Wang, L. Sun, C. Yan, Luminescent properties in relation to controllable phase and morphology of $LuBO_3:Eu^{3+}$ nano/microcrystals synthesized by hydrothermal approach, Chemistry of Materials 21 (2009) 468–475.

[14] G. Bertrand-Chadeyron, M. El-Ghozzi, D. Boyer, R. Mahiou, J. C. Cousseins, Orthoborates processed by soft routes: correlation luminescence structure, Journal of Alloys and Compounds 317/318 (2001) 183–185.

[15] Q. Dong, Y. Wang, Z. Wang, X. Yu, B. Liu, Self-Purification-Dependent Unique Photoluminescence, Properties of $YBO_3:Eu^{3+}$ nanophosphors under VUV excitation, Journal Physical Chemistry C 114 (2010) 9245–9250.

[16] J. Yang, C. Zhang, L. Wang, Z. Hou, S. Huang, H. Lian, J. Lin, Hydrothermal synthesis and luminescent properties of $LuBO_3:Tb^{3+}$ microflowers, Journal of Solid State Chemistry 181 (2008) 2672–2680.

[17] G. Jia, P.A. Tanner, C. –K. Duan, J. Dexpert-Ghys, Eu^{3+} spectroscopy: a structural probe for yttrium orthoborate phosphors, Journal Physical Chemistry C 114 (2010) 2769–2775.

[18] M. Yin, G. Corbel, M. Leblanc, E. Antic-Fidancev, J.C. Krupa, Excitation energy transfer between two 2i sites in triclinic L–$EuBO_3$ and L–$GdBO_3:Eu^{3+}$, Journal of Alloys and Compounds 302 (2000) 12–15.

[19] S. Hosokawa, Y. Tanaka, S. Iwamoto, M. Inoue, Morphology and structure of rare earth borate ($REBO_3$) synthesized by glycothermal reaction, Journal of Materials Science 43 (2008) 2276–2285.

[20] C. Qin, L. Qin, G. Chen, T. Lin, One-dimensional Eu^{3+} and Tb^{3+} doped $LaBO_3$ nanofibers: fabrication and improved luminescence performances, Materials Letters 106 (2013) 436–438.

[21] J.-C.G. Bunzli, Luminescent probes, in: J.-C.G. Bunzli, G.R. Choppin (Eds.), Lanthanide Probes in Life, Chemical and Earth Sciences, Elsevier, Amsterdam, 1989 (Chapter 7).

[22] W. Di, X. Wang, B. Chen, S. Lu, X. Zhao, Effect of OH^- on the luminescent efficiency and lifetime of Tb^{3+}-doped Yttrium orthophosphate synthesized by solution precipitation, Journal of Physical Chemistry B 109 (2005) 13154–13158.

[23] T. Ishizaka, R. Nozaki, Y. Kurokawa, Luminescence properties of Tb^{3+} and Eu^{3+}-doped alumina films prepared by the sol–gel method under various conditions and sensitized luminescence, Journal of Physics and Chemistry of Solids 63 (2002) 613–617.

[24] R. Campostrini, G. Carturan, M. Ferrari, M. Montagna, O. Pilla, Luminescence of Eu3+ ions during thermal densification of SiO_2 gel, Journal of Material Research 7 (1992) 745–753.

[25] T. Moon, S.-T. Hwang, D.-R. Jung, D. Son, C. Kim, J. Kim, M. Kang, B. Park, Hydroxyl-quenching effects on the photoluminescence properties of SnO_2:Eu^{3+} nanoparticles, Journal of Physical Chemistry C, 111, 4164–4167.

[26] J.W. Stouwdam, F.C.J.M. van Veggel, Improvement in the luminescence properties and processability of LaF_3/Ln and $LaPO_4$/Ln nanoparticles by surface modification, Langmuir 20 (2004) 11763–11771.

[27] Y.Sohn, Contour mapping 2D and 3D-photoluminescence of Au-doped one- dimensional Eu(III) and Tb(III) hydroxide and oxide nanostructures, Ceramics International, http://dx.doi.org/10.1016/j.ceramint.2013.05.016.